Supplementary Materials

Supplementary Methods

Histology

Epididymal white adipose tissue (eWAT) was fixed, embedded, and stained as previously described (1). Images were taken (Olympus FSX100 light microscope) at a magnification of 20x for CLS and 40x for CSA. Analysis was performed using Image J (National Institutes of Health). A small portion of the anterolateral LV wall was embedded in paraffin, stained with picrosirius red (2), imaged, and quantified using Cell Sense software (Olympus). Fibrosis was expressed as a percentage of the total tissue area by taking the average of four different locations (2). Intestinal tissues (duodenum and cecum) were fixed in 4% neutral buffer formalin and embedded in paraffin for periodic acid-Schiff (PAS)/Alcian blue double stain staining at 40x magnification (3,4). The length of each villus was measured from the base to the top of the villi, and the measure of crypt depth comprised of the extension between the crypt-villus junction and the base of the crypt.

Mitochondrial bioenergetics

Mitochondrial respiration and ROS emission rates were determined in permeabilized muscle fibers from the LV, as previously described (5). Briefly, whole hearts were immediately placed in ice-cold BIOPS preservation buffer and pinned open along the longitudinal side of the trabecula. Left ventricular tissue was shaved along the fiber orientation to avoid mechanical damage and placed in a separate dish of BIOPS. Fiber bundles were separated with fine-tipped forceps underneath a microscope (MX6 Stereoscope, Zeiss Microsystems, Wetzlar, Germany), incubated in 40 μg/mL saponin for 30 minutes, and washed in MiR05 respiration buffer for 15 minutes, prior to performing mitochondrial bioenergetic experiments.

LV mitochondrial respiration experiments were performed in MiR05 respiration buffer (0.5 mM EGTA, 3 mM $MgCl_2 \cdot 6H_2O$, 60 mM K-lactobionate, 10 mM KH_2PO_4, 20 mM HEPES, 20 mM taurine, 110 mM sucrose, 1 g/L FFA-free BSA; pH 7.1) in an Oxygraph high-resolution respirometer (Oroboros Instruments, Innsbruck, Austria). Temperature was set at 25˚C with constant stirring (750 rpm). ADP was titrated (25, 100, 175, 250, 500, 1000, 2000, 4000, 6000, 8000, 10000 µM ADP) in the presence of 5 mM pyruvate and 1 mM malate, followed by 10 mM glutamate, 10 mM succinate, and 10 µM cytochrome C. CPT-I-supported respiration was determined in the presence of 1 mM malate, 5 mM ADP, 60 µM P-CoA and 500 µM L-carnitine, followed by M-CoA titrations (2.5, 5, 7.5 µM M-CoA). L-carnitine sensitivity was determined by titrating L-carnitine (5, 10, 25, 50, 100, 175, 250, 350 µM L-carnitine) in the presence of 1 mM malate, 5 mM ADP, and 60 µM P-CoA. LV mitochondrial ROS experiments were performed in Buffer Z (105 mM K-MES, 30 mM KCl, 1 mM EGTA, 10 mM KH_2PO_4, 5 mM $MgCl_2 \cdot 6H_2O$, 0.005 mM pyruvate, 0.002 mM malate, 5 mg/mL BSA) with 10 µM Amplex UltraRed, 5 µM blebbistatin, 40 U/mL SOD, and 5 U/mL HRP, at 25˚C. 20 mM succinate (maximal ROS) and +100 µM ADP (submaximal) was sequentially added. All fiber bundles were recovered and freeze-dried to normalize data to fiber weight.

Mitochondrial respiration (~15-20 mg WAT) was performed in eWAT and inguinal WAT (iWAT) at 37˚C in MiR05 respiration buffer in an Oxygraph respirometer (Oroboros Instruments, Innsbruck, Austria), as previously described (1). Additions of 5 mM pyruvate + 2 mM malate, 5 mM ADP, 10 mM glutamate, 10 mM succinate, 10 µM cytochrome C, and DNP were performed. Mitochondrial ROS experiments were performed (~5 mg WAT) in a cuvette at 37˚C containing Buffer Z with 5 U/mL HRP, 10 µg/mL digitonin, 40 U/mL SOD in Buffer Z with 10 µM Amplex UltraRed. 5 mM L-carnitine and 50 µM P-CoA were added to detect lipid-supported ROS.

Fecal sequencing and metabolites

Fecal DNA was extracted using a commercially available kit (Zymo Quick-DNA Fecal/Soil Microbe Miniprep Kit). Thereafter, sample library preparation, normalization and Illumina MiSeq sequencing were conducted by the Advanced Analysis Centre (University of Guelph). Sequencing dataset was in R version 3.6.3 using the DADA2 package version 1.14.1 according to the recommended protocol (6), but with an additional amplicon sequence variant (ASV) denoising step. Classification was carried out by comparison against the Silva database, version 138 (7).

For fecal metabolite analysis, mouse fecal pellets were prepared for 1D ^{1}H NMR spectroscopy as previously described (8) with a modification to the final fecal pellet % w/v in deuterated water (D_2O; 2.24% w/v mg fecal pellet per 100 µL D_2O). Briefly, fecal pellets were weighed and D_2O was added to bring all samples to 2.24% w/v mg fecal pellet per 100 uL D_2O. Samples were then vortexed 10 minutes until homogenized, then centrifuged for 10 min, 14,000 rpm at 4°C. Supernatants were passed through a 0.2 µm PES filter. ~5 mM 3-(Trimethylsilyl)-1-propanesulfonic acid sodium salt (DSS) in deuterated water (D_2O), containing 0.1% sodium azide (Chenomx Inc.) was added to each sample to final concentration 10% v/v DSS in sample filtrate. Samples were then transferred to a 3 mm NMR tube for scanning. Each sample was scanned at 298K in a Bruker Avance III 600 MHz spectrometer with a 5 mm TCI 600 cryoprobe (Bruker, Billerica, MA, USA) at the Advanced Analysis Centre in the University of Guelph, ON, Canada according to (8), except the number of scans was increased from 32 to 1536 to increase sensitivity for the low concentration fecal filtrate samples. Sample spectra were processed and analyzed at the Advanced Analysis Centre in the University of Guelph in Chenomx NMR suite 9.0 according

to (8) with 128K zero filling and 0.2 Hz line broadening. Targeted metabolite concentrations were determined by the best fit for the peak regions within the Chenomx library of compounds.

Lipid fractions analyses

The muscle/adipose/heart tissue samples were homogenized and lipids were extracted in a chloroform-methanol solution (2:1 vol/vol) with antioxidant (9). After overnight extraction, water was added and then the samples were centrifuged (10 min., 3 000 rpm) and the lower layer was collected. Next, lipids were separated using thin-layer chromatography (TLC) on silica gel plates (Silica Plate 60, 0.25 mm; Merck, Darmstadt, Germany) with a diethyl ether/hexane/acetic acid (90:10:1, vol/vol/vol) resolving solution. Dried silica plates were visualized under ultraviolet light to identify ceramide (CER), diacylglycerol (DAG) and triacylglycerol (TAG) fractions. Thereafter, to the samples containing scrapped silica gel with lipid fractions pentadecanoic acid (C15:0; Sigma-Aldrich) or heptadecanoic acid (17:0; Sigma-Aldrich) was added as an internal standard and the samples underwent transmethylation in 14% boron trifluoride-methanol (BF_3) solution (10). The gel bands with lipid fractions were eluted with a diethyl ether/hexane (1:1, vol/vol) and a chloroform/methanol/water (5:5:1, vol/vol/vol), respectively, and then transmethylated according to Christie (11) method. Finally, the fatty acid methyl esters were extracted using pentane, which was then evaporated under a stream of nitrogen gas. Subsequently, samples were dissolved in hexane and analyzed by a Hewlett-Packard 5890 Series II gas chromatograph, an Agilent J&W CP-Sil 88 capillary column (50 m × 0.25 mm inner diameter), and a flame-ionization detector (Agilent Technologies, Santa Clara, California). The total CER, DAG and TAG PL fractions were estimated as the sum of the particular fatty acid species contents of the assessed fractions. The values were expressed as nanomoles per gram of muscle tissue dry weight.

Supplementary Tables

Supplementary Table 1 – Primary antibodies for western blot analysis.

Antibody	Dilution	Catalogue Number	Supplier
4HNE	1:1000	HNE-11s	Alpha Diagnostics
α-tubulin	1:1000	Ab7291	Abcam
ANT1	1:1000	Ab110322	Abcam
B-HAD	1:1000	Ab68321	Abcam
Catalase	1:1000	Ab16731	Abcam
COXIV	1:30,000	Ab16731	Abcam
CPT-I	1:1000	CPTI MII-A	Alpha Diagnostics
CSQ2	1:1000	Ab191564	Abcam
ERK 1&2 total	1:1000	Cs4695	Cell Signalling
ERK 1&2 phospho Ser17/Thr17	1:1000	Cs9101	Cell Signalling
JNK 1&2 total	1:1000	Cs4695	Cell Signalling
JNK 1&2 phospho Thr183/Tyr185	1:1000	Cs4671	Cell Signalling
OXPHOS	1:500	110413	MitoSciences
PLN total	1:1000	Ab2865	Abcam
PLN phospho	1:1000	Cs8496	Cell Signalling
SERCA2	1:1000	Ab2861	Abcam
SOD2	1:5000	Ab13533	Abcam
VDAC	1:1000	Ab14734	Abcam

Supplementary Table 2 – Invasive hemodynamics in FMT animals. dP/dt max, maximum rate of change of LV pressure during contraction; dP/dt min, maximum rate of change of LV pressure during relaxation; dP/dt@LVP40, rate of change of LV pressure at LV pressure equal to 40mmHg; FMT, fecal microbial transplantation; HFD, high-fat diet; LVP, left ventricle pressure. Data expressed as mean ± SEM and analyzed using unpaired Student's *t*-tests. n=10 HFD-HFD FMT, n=9 HFD-Nitrate FMT.

	HFD-HFD FMT	**HFD-HFD+Nitrate FMT**
Ejection fraction (%)	61.4 ± 2.8	68.3 ± 3.4
Fractional shortening (%)	32.3 ± 1.9	38.1 ± 2.8
Peak LVP (mmHg)	109.2 ± 1.6	111.7 ± 2.3
dP/dt max (mmHg•sec^{-1})	10314 ± 364	10428 ± 458
dP/dt@LVP40 (mmHg•sec^{-1})	9030 ± 304	8896 ± 366
dP/dt min (mmHg•sec^{-1})	-9490 ± 418	-8957 ± 427
Heart rate (bpm)	500 ± 13	510 ± 25

Supplementary Figures

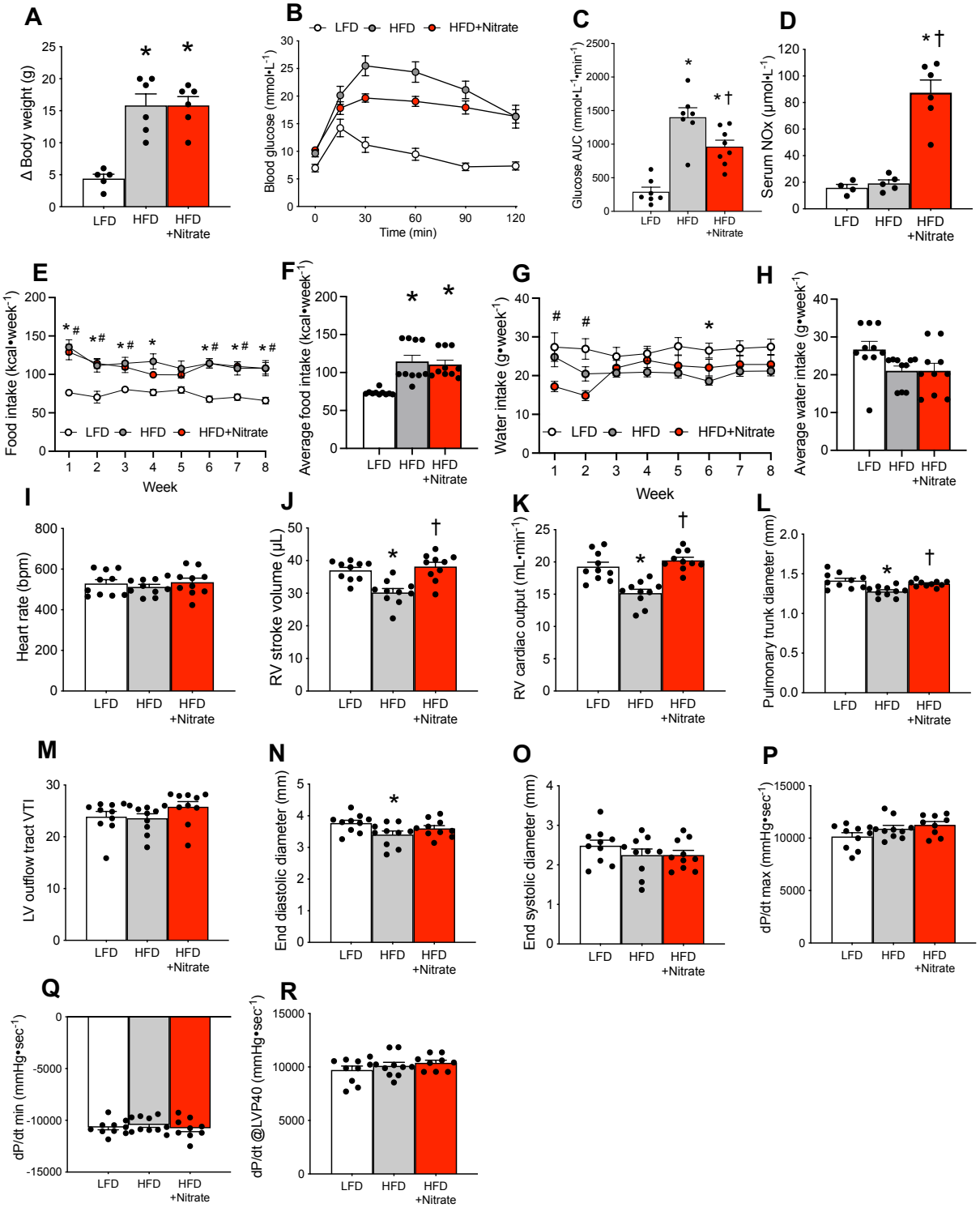

Supplementary Figure 1 – Dietary nitrate prevents HFD-induced glucose intolerance and cardiac abnormalities. Body weight gain (A), glucose tolerance (B,C), and serum NOx (D) in mice fed an LFD, HFD, or HFD+Nitrate diet. Caloric intake (E, F) was increased with HFD but did not differ with nitrate consumption. Water intake (G, H) was not influenced by nitrate supplementation. Heart rate (I) was not different between groups, while nitrate prevented the HFD-mediated decrease in RV stroke volume (J), RV cardiac output (K), and pulmonary trunk diameter (L). LV outflow tract velocity time integral (M), end diastolic diameter (N), end systolic diameter (O), dP/dt max (P), dP/dt min (Q), and dP/dt@LVP40 (R). Data expressed as mean ± SEM and analyzed using one-way ANOVA with Tukey's post-hoc test. * indicates significantly different vs. LFD. † indicates significantly different vs. HFD. # indicates significantly different for HFD+Nitrate v. LFD (E,G).

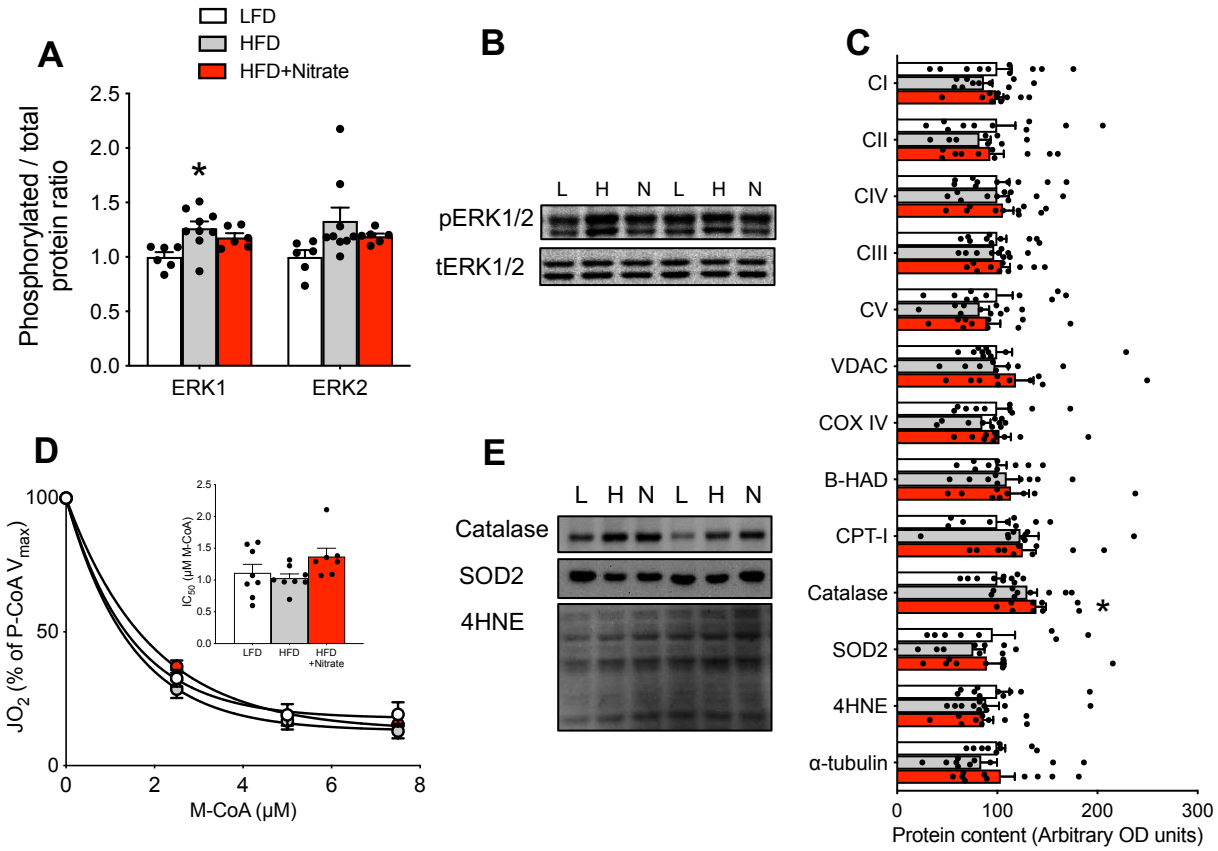

Supplementary Figure 2 – Dietary nitrate attenuates HFD-induced increases in ERK phosphorylation but does not alter protein content or M-CoA sensitivity in the LV. ERK phosphorylation (A,B) and mitochondrial protein content (C) in the LV of LFD, HFD, and HFD+Nitrate mice. Mitochondrial CPT-I sensitivity to M-CoA inhibition (D), and SOD2 and 4HNE content (E) were not altered between groups, while catalase protein content was increased in HFD+Nitrate mice. Data expressed as mean ± SEM and analyzed using one-way ANOVA with Tukey's post-hoc test. * indicates significantly different vs. LFD.

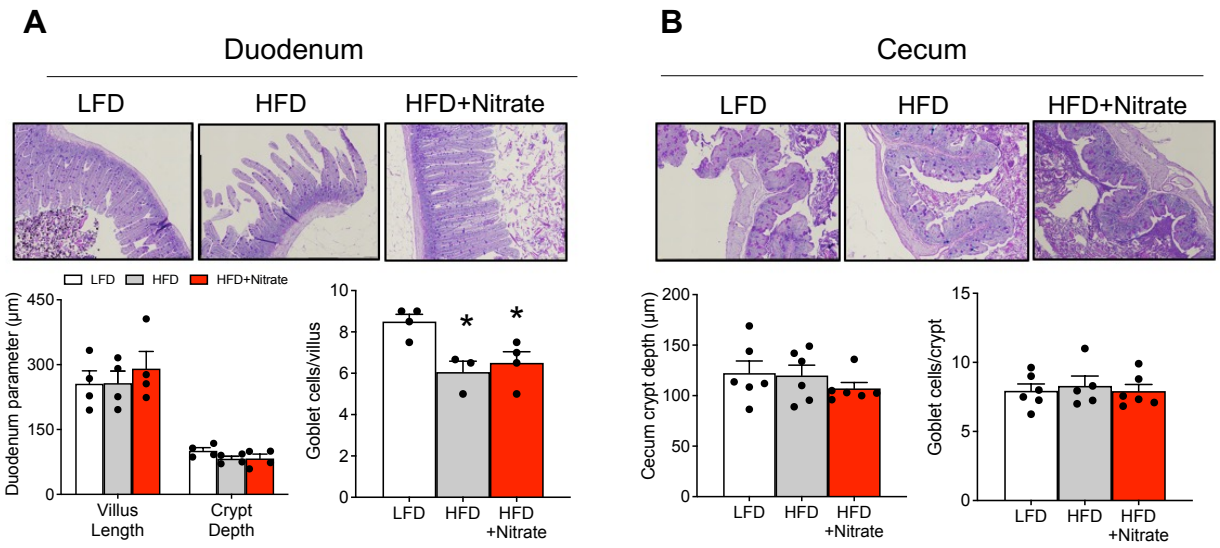

Supplementary Figure 3 – Nitrate does not influence duodenum and cecum structural morphology. Duodenal (A) and cecal (B) morphological characteristics in mice fed an LFD, HFD, or HFD+Nitrate. Data expressed as mean ± SEM and analyzed using one-way ANOVA with Tukey's post-hoc test. * indicates significantly different vs. LFD.

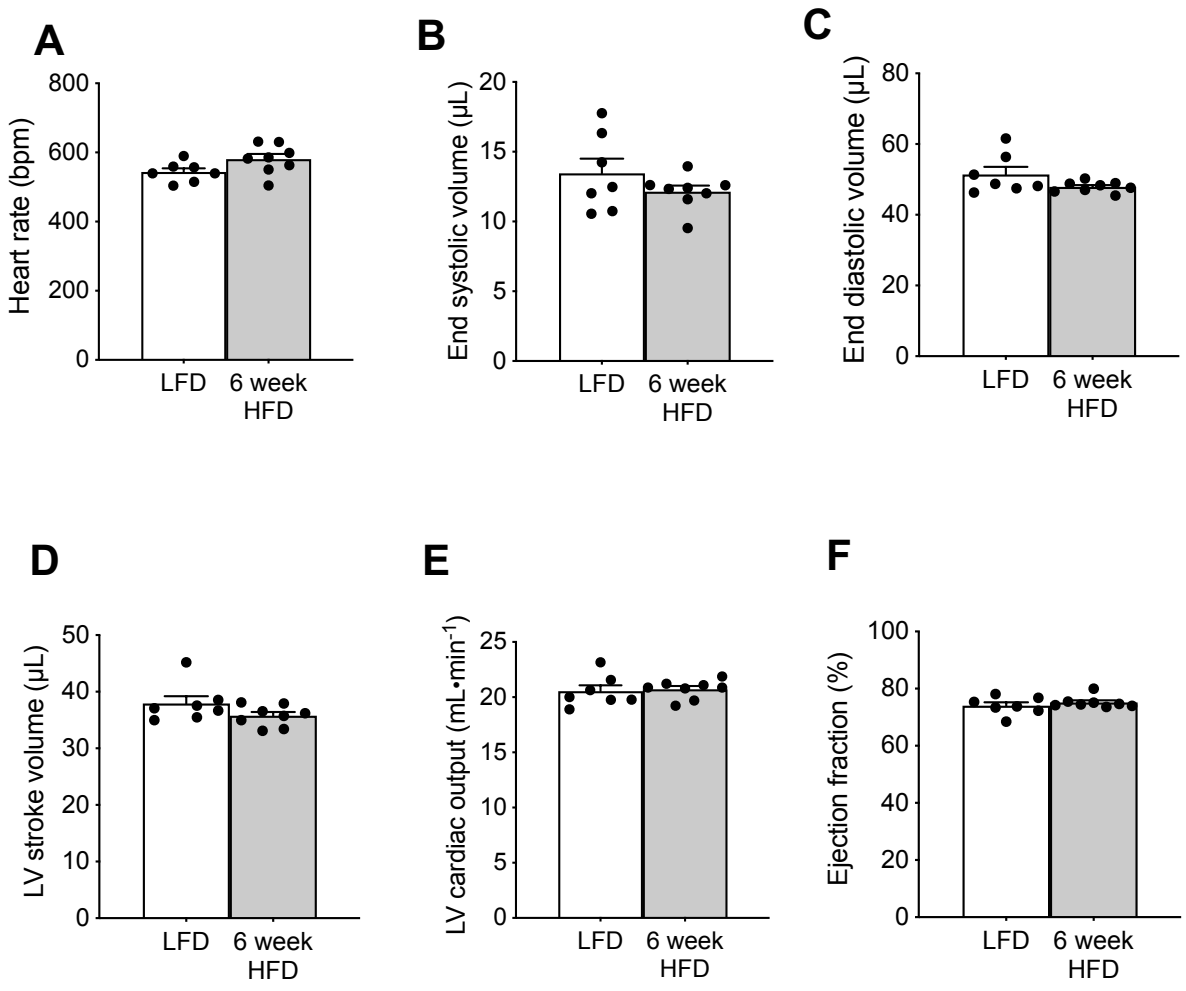

Supplementary Figure 4 – Six weeks of HFD feeding does not alter cardiac function. Heart rate (A), end systolic volume (B), end diastolic volume (C), stroke volume (D), cardiac output (E), and ejection fraction (F) in the LV of mice fed an LFD or HFD for 6 weeks. Data expressed as mean ± SEM and analyzed using unpaired two-tailed Student's *t*-tests.

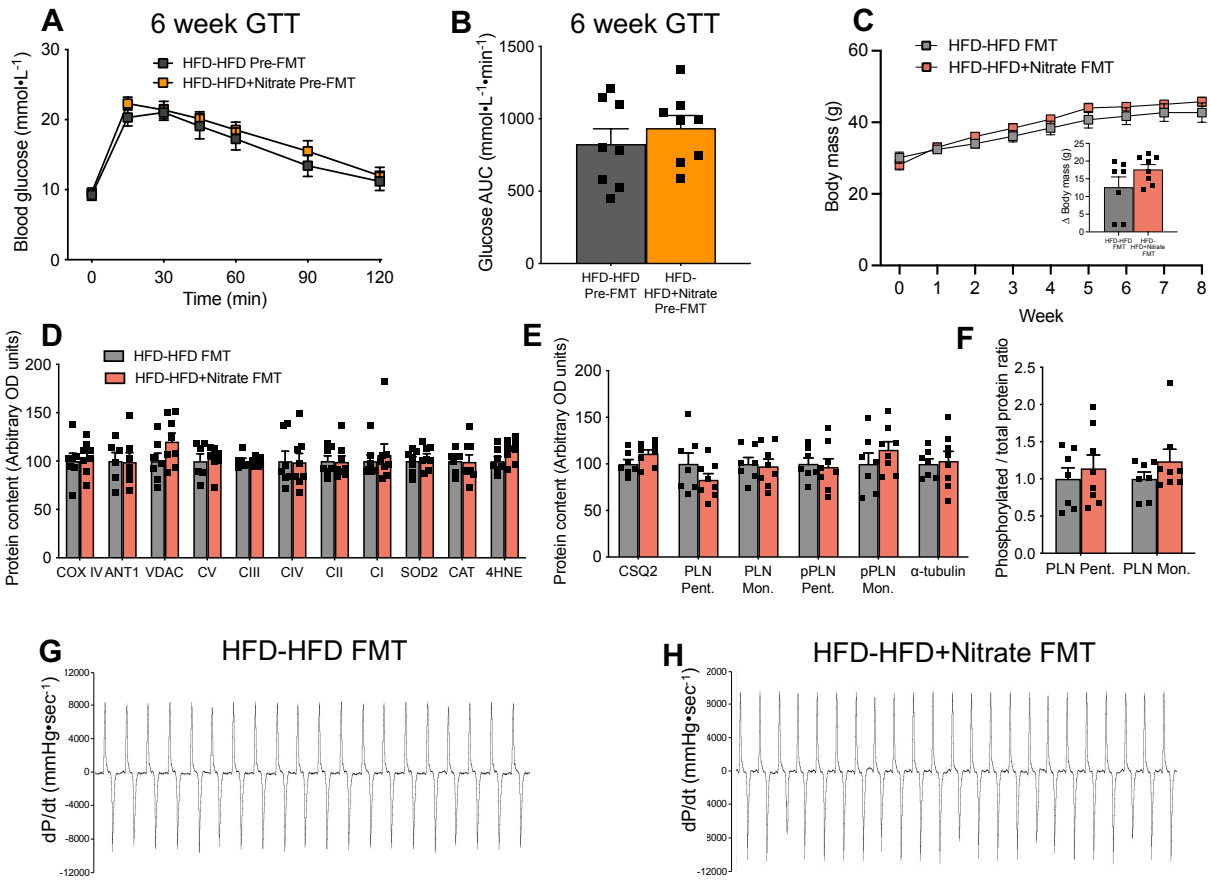

Supplementary Figure 5 – FMT from HFD+Nitrate mice does not influence protein content in the LV or dP/dt. Glucose tolerance at 6 weeks prior to FMT was similar between groups (A, B), and body mass was similar at all time-points (C). Mitochondrial and redox protein content (D), Ca^{2+}-handling proteins (E), and phosphorylated protein ratio (F) in the LV of FMT mice. Representative traces depicting dP/dt in FMT animals (G,H). Data expressed as mean ± SEM and analyzed using unpaired two-tailed Student's *t*-tests.

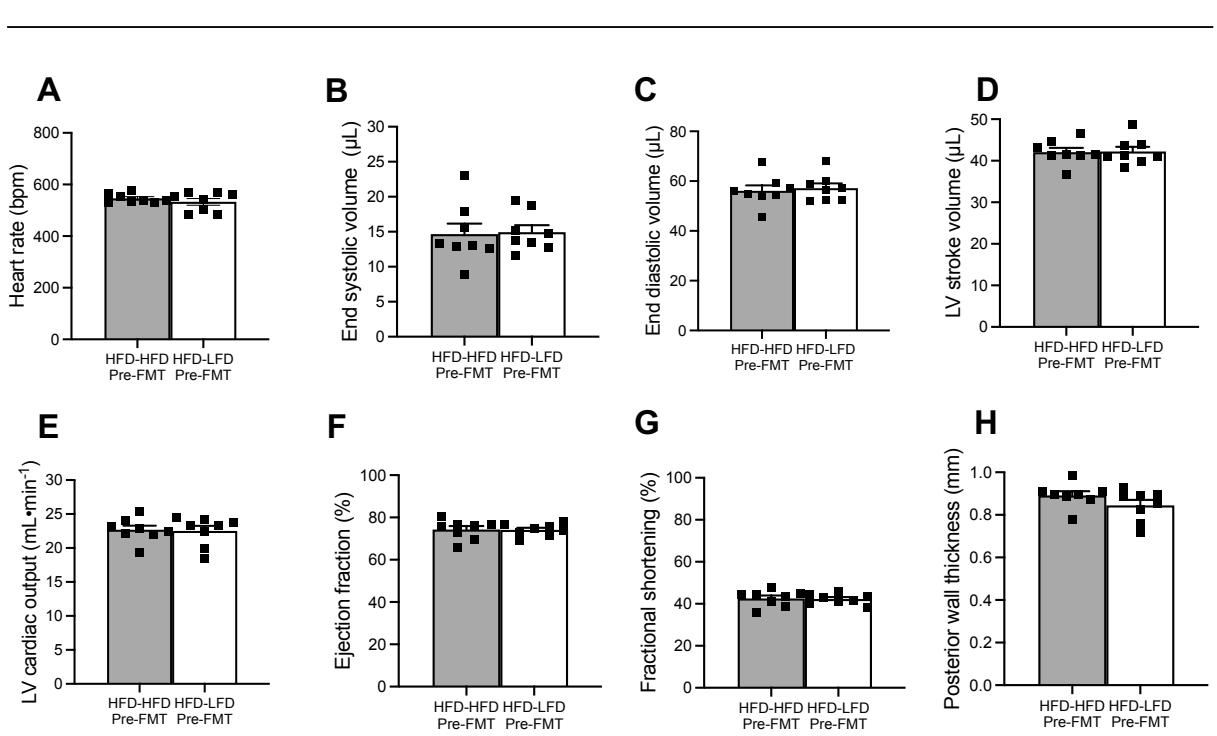

Supplementary Figure 6 – Echocardiography parameters were similar between HFD-HFD and HFD-LFD FMT groups at week 6 prior to FMT. Heart rate (A), end systolic volume (B), end diastolic volume (C), stroke volume (D), cardiac output (E) ejection fraction (F), fractional shortening (G), and posterior wall thickness (H) in mice prior to FMT. Data expressed as mean ± SEM and analyzed using unpaired two-tailed Student's *t*-tests.

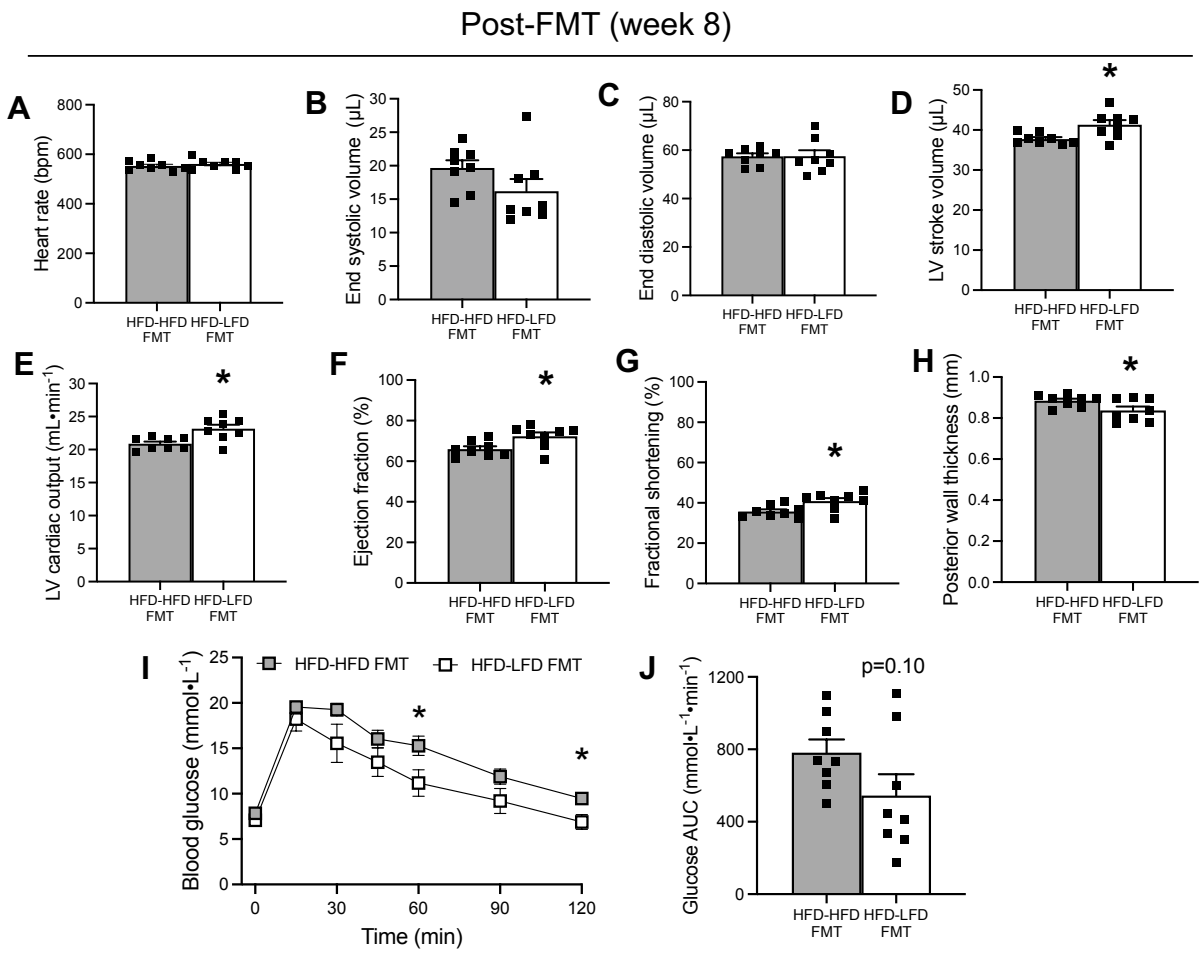

Supplementary Figure 7 – FMT from LFD donors prevents the HFD-induced impairments in cardiac function. Heart rate (A), end systolic volume (B), and end diastolic volume (C) in mice following HFD or LFD FMT. The HFD-induced decrease in stroke volume (D), cardiac output (E) ejection fraction (F), and fractional shortening (G); and increase in posterior wall thickness (H), was prevented by LFD FMT. In addition, LFD FMT trended towards greater glucose tolerance (I, J) compared to HFD FMT. Data expressed as mean ± SEM and analyzed using unpaired two-tailed Student's *t*-tests. * indicates significantly different vs. HFD-HFD FMT.

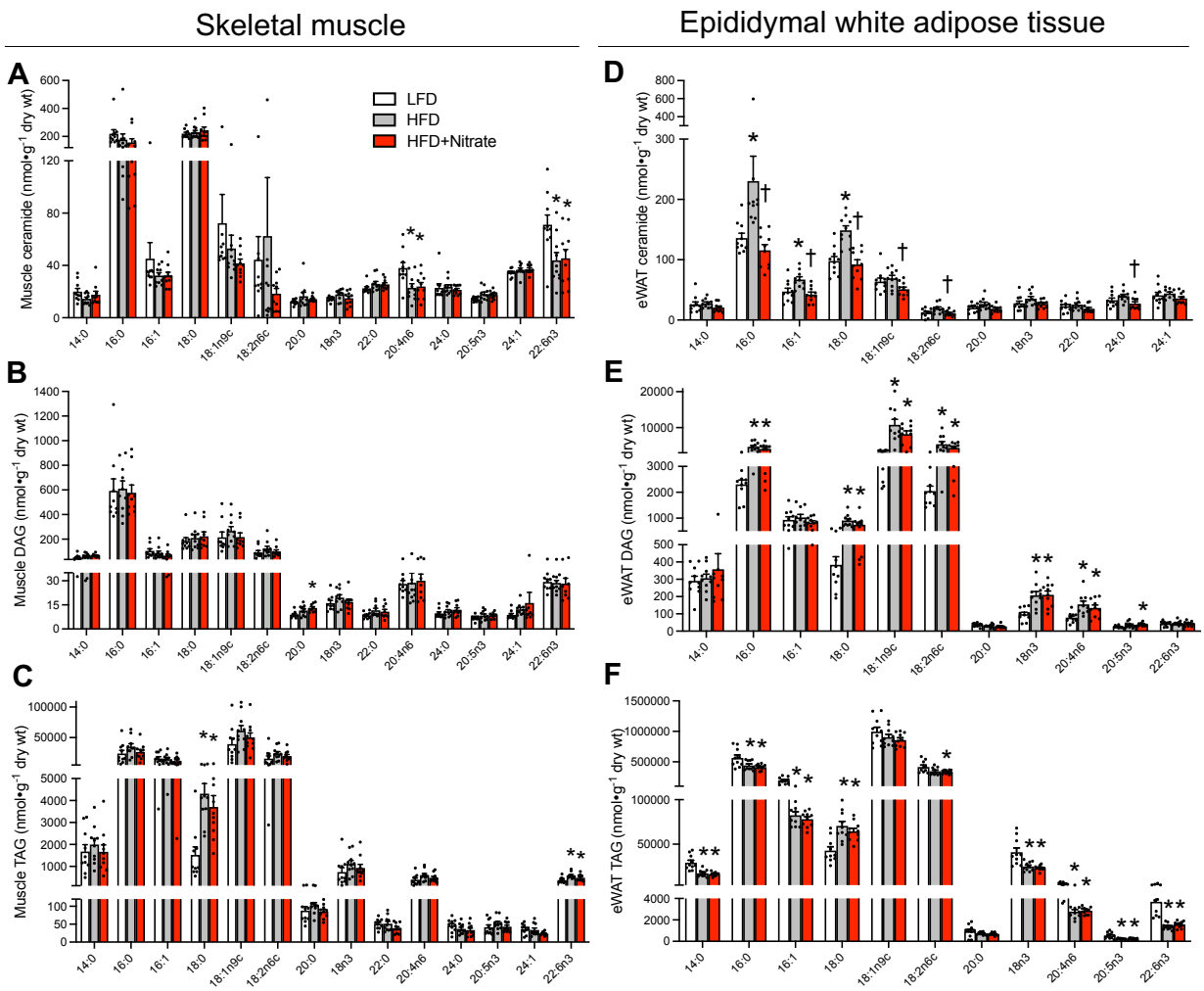

Supplementary Figure 8 – Nitrate supplementation prevents HFD-induced increases in ceramide species within eWAT. Ceramide (A), DAG (B), and TAG (C) species in skeletal muscle. Ceramide (D), DAG (E), and TAG (F) species in eWAT. Data expressed as mean ± SEM and analyzed using one-way ANOVA with Tukey's post-hoc test. * indicates significantly different vs. LFD. † indicates significantly different vs. HFD.

References

1. Paglialunga S, Ludzki A, Root-McCaig J, Holloway GP. In adipose tissue, increased mitochondrial emission of reactive oxygen species is important for short-term high-fat diet-induced insulin resistance in mice. Diabetologia. 2015;58:1071–80.
2. Barbeau PA, Holloway TM, Whitfield J, Baechler BL, Quadrilatero J, van Loon LJ, et al. α -Linolenic acid and exercise training independently, and additively, decrease blood pressure and prevent diastolic dysfunction in obese Zucker rats. J Physiol. 2017;13:4351–64.
3. Lee JC, Lee HY, Kim TK, Kim MS, Park YM, Kim J, et al. Obesogenic diet-induced gut barrier dysfunction and pathobiont expansion aggravate experimental colitis. PLoS One. 2017;12(11):1–27.
4. Mao J, Hu X, Xiao Y, Yang C, Ding Y, Hou N, et al. Overnutrition stimulates intestinal epithelium proliferation through β-catenin signaling in obese mice. Diabetes. 2013;62(11):3736–46.
5. Monaco CM, Miotto PM, Huber JS, Loon LJC Van, Simpson JA, Holloway GP. Sodium nitrate supplementation alters mitochondrial H2O2 emission but does not improve mitochondrial oxidative metabolism in the heart of healthy rats. Am J Physiol Regul Integr Comp Physiol. 2018;315:R191–204.
6. Callahan BJ, McMurdie PJ, Rosen MJ, Han AW, Johnson AJA, Holmes SP. DADA2: High-resolution sample inference from Illumina amplicon data. Nat Methods. 2016;13(7):581–3.
7. Quast C, Pruesse E, Yilmaz P, Gerken J, Schweer T, Yarza P, et al. The SILVA ribosomal RNA gene database project: improved data processing and web-based tools. Nucleic Acids Res. 2013;41(D1):D590–6.
8. Ganobis CM, Al-Abdul-Wahid MS, Renwick S, Yen S, Carriero C, Aucoin MG, et al. 1D 1H NMR as a Tool for Fecal Metabolomics. Curr Protoc Chem Biol. 2020;12(3):e83.
9. Bligh, E.G. and Dyer WJ. A rapid method of total lipid extraction and purification. Can J Biochem Physiol. 1959;37(8):911–7.
10. Morrison WR, Smith LM. Preparation of fatty acid methyl esters and dimethylacetals from lipids with boron fluoride–methanol. J Lipid Res. 1964;5(4):600–8.
11. Christie WW. A simple procedure for rapid transmethylation of glycerolipids and cholesteryl esters. J Lipid Res. 1982;23(7):1072–5.